

Lattice QCD study of color correlations between quarks in static multiquark systems

Toru T. Takahashi

National Institute of Technology, Gunma College, Maebashi, Gunma 371-8530, Japan

Yoshiko Kanada-En'yo

Department of Physics, Kyoto University, Sakyo, Kyoto 606-8502, Japan

(Dated: December 29, 2025)

We study the color correlation between two static quarks in 3Q (QQQ) and 4Q ($QQ\bar{Q}\bar{Q}$) multiquark systems at $T = 0$ based on the reduced two-body density matrices ρ in color space. We perform quenched lattice QCD calculations with the Coulomb gauge adopting the standard Wilson gauge action, and the spatial volume is $L^3 = 32^3$ at $\beta = 5.8$, which corresponds to the lattice spacing $a = 0.14$ fm and the system volume $L^3 = 4.5^3$ fm 3 . We evaluate the two-body color density matrix ρ of static quarks, and investigate the dependence of color correlations on the quarks' spatial configuration. As a result, we find that the color correlations depend on the minimal path length along a flux tube which connects two quarks under consideration. The color correlation between quarks quenches because of color leak into the gluon field (flux tube) and finally approaches the random color configuration in the large distance limit. We find a “universality” in the flux-tube path length dependence of the color leak for 2Q, 3Q, and 4Q ground-state systems.

I. INTRODUCTION

QuantumChromoDynamics (QCD) is the fundamental theory of the strong interaction, and quarks are all confined in a totally color-singlet hadronic cluster due to the color confinement phenomenon caused by QCD [1]. There have been a lot of attempts to clarify the color confining nature of QCD, and its nonperturbative dynamics is still attracting great interest. In color singlet hadronic clusters, quarks' color flows into in-between gluon field forming a confining flux tube among quarks [2–9]. The in-between flux tube is a colored gluonic object created by end-point color sources, quarks, and total systems are kept color singlet by quarks and gluons [5, 6].

In Refs. [10–12], we studied color correlations in two static quark systems ($Q\bar{Q}$), and found that the color charge initially associated with quarks flows into the interquark region, and forms a confining flux tube as the total system size is enlarged. This color transfer to the flux tube can be regarded as a color charge leak from quarks to the gluon fields, and is quantified as the color screening effect among quarks. When quarks are located at distances close to each other, color from a quark is absorbed by other quarks without any loss, and color leak into gluon fields (flux tube) hardly occurs. In this case, the color correlation among quarks is maximal. As the system size is enlarged, a physical gluonic flux tube grows and quarks' color is screened inside the tube, which in turn weakens the quarks' color correlation. This correlation quench is expressed as a mixture of a random color contribution into quarks' color configuration, in which *all the color combinations of the quark pair equally contribute* [10–12]. At the large system size limit, the correlation disappears and the quarks' color configuration approaches a random color configuration [10–12]. This color transfer mechanism, from quarks to in-between gluons, is also found in a $Q\bar{Q}$ system accompanied by gluonic excitations [12].

While we have so far focused on systems consisting of static quark and antiquark ($Q\bar{Q}$), quarks' color correlations in multiquark systems are also of great interest. In multiquark systems, there can appear flux tubes that have “junctions” [3, 4, 7–9], and the color structure and the color flow inside hadronic clusters would be more complicated than simple $Q\bar{Q}$ cases. In this paper, we define the two-body reduced color density matrix ρ for 3Q (QQQ) and 4Q ($QQ\bar{Q}\bar{Q}$) systems, and investigate the color structure of the multiquark systems. According to the ansatz for the reduced density matrix ρ proposed in Ref. [10], we clarify the color correlation of two quarks inside the multiquark systems.

In Sec. II, we give the formalism to compute the reduced density matrix ρ of multiquark systems. The details of numerical calculations and ansatz for ρ are also shown in Sec. II. Results are presented in Sec. III, Sec. IV, and Sec. V. Sec. VI is devoted to the summary and concluding remarks.

II. FORMALISM

A. reduced 2-body density matrix and quarks' color correlation

We investigate the color correlation between two static (anti)quarks via the two-body density matrix ρ evaluated in terms of quarks' color configuration. A density matrix ρ defined in such a way corresponds to the reduced density matrix obtained by integrating out the other degrees of freedom (d.o.f.) (e.g., gluonic d.o.f.) in the full density matrix.

In the following, we exemplify the formalism using quarks Q_i . When a system containing antiquarks is considered, readers should substitute Q_i with \bar{Q}_i as appropriate.

For an N -quark (NQ) system, we choose two quarks of

them in order to investigate the color correlation of quark pairs in NQ systems. A full density operator $\hat{\rho}_{\text{full}}(\mathcal{R})$ for an NQ system is defined as

$$\hat{\rho}_{\text{full}}(\mathcal{R}) = |NQ(\mathcal{R})\rangle\langle NQ(\mathcal{R})|. \quad (1)$$

Here $|NQ(\mathcal{R})\rangle$ represents a quantum state of an NQ system. \mathcal{R} is a vector set defined as $\mathcal{R} \equiv \{\vec{r}_1, \vec{r}_2, \vec{r}_3, \dots\}$, where the vector \vec{r}_i denotes the i -th quark's (Q_i 's) spatial position. When we measure the color correlation between the i - and j -th quarks, Q_k ($k \neq i, j$) are all “spectator” quarks in the sense that we do not see their colors, and that their dynamics are traced out. Gluon fields' color is not seen either, and is also traced out in the lattice QCD simulation. Then, the quantum state we will find for the target quark pair ($Q_i Q_j$ pair) is expressed by the reduced density operator

$$\hat{\rho}(\mathcal{R}) = \int \mathcal{D}Q' \mathcal{D}G \langle Q'G | \hat{\rho}_{\text{full}}(\mathcal{R}) | Q'G \rangle. \quad (2)$$

Here, Q' represents the d.o.f. for all the spectator quarks other than Q_i and Q_j ($|Q' \rangle \equiv \Pi_{k \neq i, j} |Q_k(\vec{r}_k)\rangle$), and G denotes all the gluonic d.o.f. Note that the reduced density operator $\hat{\rho}(\mathcal{R})$ still depends on the spatial positions of spectator quarks, \vec{r}_k ($k \neq i, j$). The matrix elements $\rho(\mathcal{R})_{ab,cd}$ of the reduced density operator, where a and c (b and d) are quark's color indices, are expressed as

$$\rho(\mathcal{R})_{ab,cd} = \langle Q_i^a(\vec{r}_i) Q_j^b(\vec{r}_j) | \hat{\rho}(\mathcal{R}) | Q_i^c(\vec{r}_i) Q_j^d(\vec{r}_j) \rangle. \quad (3)$$

$|Q_i^c(\vec{r}_i) Q_j^d(\vec{r}_j)\rangle$ represents a state in which the i - and j -th quarks located at \vec{r}_i and \vec{r}_j have color indices c and d , respectively. In this case, k -th quarks ($k \neq i, j$) are all spectators. In $\rho(\mathcal{R})_{ab,cd}$, we omit the quarks' indices, i and j , as long as there is no misunderstanding.

Then, $\rho(\mathcal{R})$ is an $N_c \times N_c$ square matrix. The density matrix $\rho(\mathcal{R})$ is evaluated using only target quarks' color d.o.f., and does not explicitly contain spectator quarks' and gluon's color d.o.f. in this construction: the spectator quarks' and gluonic d.o.f. are “integrated out” in the lattice calculation, and $\rho(\mathcal{R})$ can be regarded as a reduced density matrix [10].

B. Ansatz for reduced density matrix $\rho_{ab,cd}(\mathcal{R})$

In the series of our papers [10–12], we investigated the color structure of quark and antiquark in static $Q\bar{Q}$ systems with and without gluonic excitations. As a result, we found that the color correlation is randomized as the interquark distance R increases for both systems. In a ground-state QQ system with no gluonic excitation, the color configuration of a $Q\bar{Q}$ pair can be well represented by the density operator [10, 11]

$$\hat{\rho}^{\text{ansatz}}(R) = F_1(R) \hat{\rho}_1 + (1 - F_1(R)) \hat{\rho}^{\text{rand}}, \quad (4)$$

where R is the interquark distance. Here, $\hat{\rho}_1 = |\mathbf{1}\rangle\langle\mathbf{1}|$ is a density operator for a $Q\bar{Q}$ pair that forms a purely color

singlet configuration in the Coulomb gauge, and $\hat{\rho}^{\text{rand}}$ is that for a random color state where one singlet state and eight octet states enter with equal weights. The “initial” color configuration of a $Q\bar{Q}$ pair at $R \sim 0$ was found to be color singlet, and it leads to $F_1(R) \sim 1$. On the other hand, when the $Q\bar{Q}$ distance R is large, the color configuration is randomized and $F_1(R)$ approaches zero.

This ansatz with $\hat{\rho}^{\text{rand}}$ is also applicable for $Q\bar{Q}$ systems with gluonic excitations ($Q\bar{Q}G$ systems). By replacing the initial color configuration $\hat{\rho}_1$ with $\hat{\rho}_8 = \frac{1}{8} \sum_i |\mathbf{8}_i\rangle\langle\mathbf{8}_i|$ representing the color octet state, which “initially” dominates the $Q\bar{Q}G$ system at $R \sim 0$, the color configuration of a $Q\bar{Q}$ pair in a $Q\bar{Q}G$ system can be expressed by the density operator [12]

$$\hat{\rho}^{\text{ansatz}}(R) = F_8(R) \hat{\rho}_8 + (1 - F_8(R)) \hat{\rho}^{\text{rand}}. \quad (5)$$

From these observations, $F_1(R)$ and $F_8(R)$ in the ansatz are considered to be a *residual rate of the maximally correlated configuration* of a (hybrid) $Q\bar{Q}$ pair, which is expected when no gluon flux tube is present at $R \rightarrow 0$. In fact, at $R \rightarrow 0$, the color flowing out of one quark is fully absorbed by the antiquark with no color leak, and the $Q\bar{Q}$ color correlation is maximized. As a physical flux tube grows between quarks, the color from quarks is absorbed also by in-between gluons, and the color correlation between end-point quarks is weakened. The exponential decay of the “residual rate” $F_1(R)$ and $F_8(R)$ implies quarks' color screening by in-between gluons, and it was investigated in detail in the previous papers [10–12].

By analogy with the previous results of $Q\bar{Q}$ systems, we consider the case of multiquark systems. When all the quarks are located in close to each other and there is no color leak to a gluon flux tube, any two quarks in multiquark systems are expected to form “maximally correlated” (MC) color states depending on a system under investigation, and the random configuration would enter as in-between gluon flux tubes grow. Note that this MC state is nothing but a quarks' color configuration that appears when no color leak from quarks to gluon fields occurs at $\mathcal{R} \rightarrow 0$ ($|r_i| \rightarrow 0$ for all i). With the density operator $\hat{\rho}^{\text{MC}}$ for this MC state, we introduce the color density operator $\hat{\rho}^{\text{ansatz}}$ for a quark pair as

$$\hat{\rho}^{\text{ansatz}}(\mathcal{R}) = F_{\text{MC}}(\mathcal{R}) \hat{\rho}^{\text{MC}} + (1 - F_{\text{MC}}(\mathcal{R})) \hat{\rho}^{\text{rand}}. \quad (6)$$

Here, $F_{\text{MC}}(\mathcal{R})$ represents the “residual rate” of the MC state expected when there is no color leak to gluon flux tubes at $\mathcal{R} \rightarrow 0$. The color configuration of a quark pair for any \mathcal{R} can be solely represented by $F_{\text{MC}}(\mathcal{R})$ in this ansatz.

1. QQ color correlation in 3Q and 4Q systems

First, we consider the case when we measure the color correlation between two quarks (QQ) in multiquark (3Q and 4Q) systems. A color configuration of any QQ pair is

decomposed into color antitriplet and sextet states. Let $\hat{\rho}_{\bar{\mathbf{3}}_i}$ and $\hat{\rho}_{\mathbf{6}_i}$ be the density operators for color antitriplet states $|\bar{\mathbf{3}}_i\rangle$ and sextet states $|\mathbf{6}_i\rangle$ in the Coulomb gauge respectively expressed as

$$\hat{\rho}_{\bar{\mathbf{3}}_i} = |\bar{\mathbf{3}}_i\rangle\langle\bar{\mathbf{3}}_i| \quad (i = 1 \sim 3), \quad (7)$$

$$\hat{\rho}_{\mathbf{6}_i} = |\mathbf{6}_i\rangle\langle\mathbf{6}_i| \quad (i = 1 \sim 6). \quad (8)$$

These density operators can be expressed in a matrix form that diagonalizes $\hat{\rho}_{\bar{\mathbf{3}}_i}$ and $\hat{\rho}_{\mathbf{6}_i}$. For example, for $i = 2$,

$$\hat{\rho}_{\bar{\mathbf{3}}_i} = \text{diag}(0, 1, 0, \dots, 0)_{\alpha}. \quad (9)$$

Here, the subscript “ α ” means that the matrix is expressed in terms of QQ ’s color representation with the vector set of $\alpha = \{|\bar{\mathbf{3}}_1\rangle, \dots, |\mathbf{6}_1\rangle, \dots, |\mathbf{6}_6\rangle\}$.

Taking into account the color $SU(3)$ symmetry, it is convenient to define the averaged density operators $\hat{\rho}_{\bar{\mathbf{3}}}$ and $\hat{\rho}_{\mathbf{6}}$ for antitriplet and sextet states as

$$\hat{\rho}_{\bar{\mathbf{3}}} = \frac{1}{3} \sum_{i=1}^3 \hat{\rho}_{\bar{\mathbf{3}}_i}, \quad \hat{\rho}_{\mathbf{6}} = \frac{1}{6} \sum_{i=1}^6 \hat{\rho}_{\mathbf{6}_i}. \quad (10)$$

As the interquark distance increases, an uncorrelated state, *i.e.*, a randomized-color state, mixes in $\rho(\mathcal{R})$ due to the color screening effect by in-between gluons. Such a random-color state contains all the N_c^2 components with equal weights, and its density operator is given as

$$\hat{\rho}^{\text{rand}} = \frac{1}{N_c^2} \left(\sum_{i=1}^3 \hat{\rho}_{\bar{\mathbf{3}}_i} + \sum_{i=1}^6 \hat{\rho}_{\mathbf{6}_i} \right) \quad (11)$$

$$= \frac{1}{N_c^2} \hat{I} = \text{diag} \left(\frac{1}{N_c^2}, \frac{1}{N_c^2}, \dots, \frac{1}{N_c^2} \right)_{\alpha}. \quad (12)$$

We are mainly interested in the ground-state 3Q and 4Q systems, and their color structures will be $([Q_1 Q_2] Q_3)$ and $([Q_1 Q_2] [\bar{Q}_3 \bar{Q}_4])$ when all the quarks are close to each other at $\mathcal{R} \rightarrow 0$. Here, the square and curly brackets respectively show that inside quarks form a color (anti)triplet and singlet configuration. In this case, any QQ pair is considered to form a color-antitriplet state ($|\bar{\mathbf{3}}_i\rangle$) corresponding to the MC configuration in both systems, hence we choose $\hat{\rho}_{\bar{\mathbf{3}}}$ for $\hat{\rho}^{\text{MC}}$ in Eq. (6) to measure QQ correlations in 3Q and 4Q systems. Letting the residual rate of the MC color antitriplet state be $F_{\bar{\mathbf{3}}}(\mathcal{R})$ and the fraction of the random contribution be $(1 - F_{\bar{\mathbf{3}}}(\mathcal{R}))$, the density operator for a spatial configuration \mathcal{R} in this ansatz is written as

$$\hat{\rho}_{0, \bar{\mathbf{3}}}^{\text{ansatz}}(\mathcal{R}) = F_{\bar{\mathbf{3}}}(\mathcal{R}) \hat{\rho}_{\bar{\mathbf{3}}} + (1 - F_{\bar{\mathbf{3}}}(\mathcal{R})) \hat{\rho}^{\text{rand}}. \quad (13)$$

Here, the subscript $(0, \bar{\mathbf{3}})$ means that the density operator $\hat{\rho}_{0, \bar{\mathbf{3}}}^{\text{ansatz}}(\mathcal{R})$ is dominated by the color antitriplet contribution $\hat{\rho}_{\bar{\mathbf{3}}}$ at $\mathcal{R} \rightarrow 0$. The matrix form $\rho(\mathcal{R})_{\alpha}$ of $\hat{\rho}_{0, \bar{\mathbf{3}}}^{\text{ansatz}}(\mathcal{R})$ is expressed as

$$\hat{\rho}_{0, \bar{\mathbf{3}}}^{\text{ansatz}}(\mathcal{R}) = F_{\bar{\mathbf{3}}}(\mathcal{R}) \hat{\rho}_{\bar{\mathbf{3}}} + (1 - F_{\bar{\mathbf{3}}}(\mathcal{R})) \hat{\rho}^{\text{rand}} \quad (14)$$

$$= \left(F_{\bar{\mathbf{3}}}(\mathcal{R}) + \frac{3}{N_c^2} (1 - F_{\bar{\mathbf{3}}}(\mathcal{R})) \right) \hat{\rho}_{\bar{\mathbf{3}}} + \left(\frac{6}{N_c^2} (1 - F_{\bar{\mathbf{3}}}(\mathcal{R})) \right) \hat{\rho}_{\mathbf{6}} \quad (15)$$

$$= \text{diag} \left(\frac{1}{3} F_{\bar{\mathbf{3}}}(\mathcal{R}) + \frac{1}{N_c^2} (1 - F_{\bar{\mathbf{3}}}(\mathcal{R})), \dots, \frac{1}{N_c^2} (1 - F_{\bar{\mathbf{3}}}(\mathcal{R})), \dots \right)_{\alpha} \quad (16)$$

$$\equiv \text{diag} \left(\rho(\mathcal{R})_{\bar{\mathbf{3}}_1, \bar{\mathbf{3}}_1}, \dots, \rho(\mathcal{R})_{\mathbf{6}_1, \mathbf{6}_1}, \dots \right)_{\alpha}. \quad (17)$$

In this ansatz,

$$\begin{cases} \rho(\mathcal{R})_{\bar{\mathbf{3}}_1, \bar{\mathbf{3}}_1} = \rho(\mathcal{R})_{\bar{\mathbf{3}}_2, \bar{\mathbf{3}}_2} = \rho(\mathcal{R})_{\bar{\mathbf{3}}_3, \bar{\mathbf{3}}_3} \\ \rho(\mathcal{R})_{\mathbf{6}_1, \mathbf{6}_1} = \rho(\mathcal{R})_{\mathbf{6}_2, \mathbf{6}_2} = \dots = \rho(\mathcal{R})_{\mathbf{6}_6, \mathbf{6}_6} \\ \rho(\mathcal{R})_{\mathbf{a}, \mathbf{b}} = 0 \quad (\text{for } \mathbf{a} \neq \mathbf{b}) \end{cases} \quad (18)$$

and the normalization condition

$$\text{Tr } \rho(\mathcal{R}) = \rho_{\bar{\mathbf{3}}}(\mathcal{R}) + \rho_{\mathbf{6}}(\mathcal{R}) = 1 \quad (19)$$

are satisfied at any \mathcal{R} . Here, $\rho_{\bar{\mathbf{3}}}(\mathcal{R})$ and $\rho_{\mathbf{6}}(\mathcal{R})$ are the

summations of the diagonal matrix elements,

$$\rho_{\bar{\mathbf{3}}}(\mathcal{R}) \equiv \sum_{i=1}^3 \rho(\mathcal{R})_{\bar{\mathbf{3}}_i, \bar{\mathbf{3}}_i}, \quad \rho_{\mathbf{6}}(\mathcal{R}) \equiv \sum_{i=1}^6 \rho(\mathcal{R})_{\mathbf{6}_i, \mathbf{6}_i}, \quad (20)$$

which indicate the antitriplet and sextet components. We directly compute $\rho_{\bar{\mathbf{3}}}$ and $\rho_{\mathbf{6}}$ using lattice QCD calculations, and the residual rate $F_{\bar{\mathbf{3}}}(\mathcal{R})$ can be extracted from $\rho_{\bar{\mathbf{3}}}(\mathcal{R})$ or $\rho_{\mathbf{6}}(\mathcal{R})$ as

$$F_{\bar{\mathbf{3}}}(\mathcal{R}) = 1 - \frac{N_c^2}{6} \rho_{\mathbf{6}}(\mathcal{R}). \quad (21)$$

Indeed, it was found that this ansatz reproduces the density matrix element for the ground-state $Q\bar{Q}$ system evaluated by lattice QCD calculation with a very good accuracy [10].

2. $Q\bar{Q}$ color correlation in 4Q systems

The color configuration of a $Q\bar{Q}$ pair in 4Q ($QQ\bar{Q}\bar{Q}$) systems is classified into singlet and octet color configurations, $|\mathbf{1}\rangle$ and $|\mathbf{8}_i\rangle$. Then we define the density operators for a pair forming a color singlet state $|\mathbf{1}\rangle$ and an octet state $|\mathbf{8}_i\rangle$ in the Coulomb gauge as

$$\hat{\rho}_{\mathbf{1}} = |\mathbf{1}\rangle\langle\mathbf{1}|, \quad \hat{\rho}_{\mathbf{8}_i} = |\mathbf{8}_i\rangle\langle\mathbf{8}_i| \quad (i = 1 \sim N_c^2 - 1). \quad (22)$$

As before, we define the averaged density operator $\hat{\rho}_{\mathbf{8}}$ as

$$\hat{\rho}_{\mathbf{8}} = \frac{1}{N_c^2 - 1} \sum_{i=1}^{N_c^2 - 1} \hat{\rho}_{\mathbf{8}_i}. \quad (23)$$

In the case when we measure the color correlation in

side a $Q\bar{Q}$ pair in a 4Q system, the “initial” MC color configuration of a $Q\bar{Q}$ pair would be neither $|\mathbf{1}\rangle$ nor $|\mathbf{8}_i\rangle$, but a combination of them. Especially when four quarks form a “genuine” multiquark state ($[Q_1Q_2][\bar{Q}_3\bar{Q}_4]$), $\hat{\rho}$ in Eq.(6) would be [8]

$$\hat{\rho}^{\text{MC}} = \frac{1}{3}\hat{\rho}_{\mathbf{1}} + \frac{2}{3}\hat{\rho}_{\mathbf{8}} \equiv \hat{\rho}^{\text{combi}}, \quad (24)$$

leading to the ansatz for 4Q systems

$$\hat{\rho}_{0,c}^{\text{ansatz}}(\mathcal{R}) = F_c(\mathcal{R})\hat{\rho}^{\text{combi}} + (1 - F_c(\mathcal{R}))\hat{\rho}^{\text{rand}} \quad (25)$$

$$= F_c(\mathcal{R}) \left(\frac{1}{3}\hat{\rho}_{\mathbf{1}} + \frac{2}{3}\hat{\rho}_{\mathbf{8}} \right) + (1 - F_c(\mathcal{R}))\hat{\rho}^{\text{rand}}. \quad (26)$$

Here, the subscript $(0, c)$ means that the density operator $\hat{\rho}_{0,c}^{\text{ansatz}}(\mathcal{R})$ is expressed by the residual rate $F_c(\mathcal{R})$ of the MC color configuration $\hat{\rho}^{\text{combi}}$, and $\hat{\rho}^{\text{combi}}$ dominates $\hat{\rho}_{0,c}^{\text{ansatz}}(\mathcal{R})$ at $\mathcal{R} \rightarrow 0$ corresponding to $F_c(\mathcal{R}) \sim 1$. In the matrix form β expressed with the vector set of $\beta = \{|\mathbf{1}\rangle, |\mathbf{8}_1\rangle, \dots, |\mathbf{8}_8\rangle\}$, $\hat{\rho}_{0,c}^{\text{ansatz}}(\mathcal{R})$ can be explicitly expressed as

$$\hat{\rho}_{0,c}^{\text{ansatz}}(\mathcal{R}) = F_c(\mathcal{R}) \left(\frac{1}{3}\hat{\rho}_{\mathbf{1}} + \frac{2}{3}\hat{\rho}_{\mathbf{8}} \right) + (1 - F_c(\mathcal{R}))\hat{\rho}^{\text{rand}} \quad (27)$$

$$= \left(\frac{1}{3}F_c(\mathcal{R}) + \frac{1}{N_c^2}(1 - F_c(\mathcal{R})) \right) \hat{\rho}_{\mathbf{1}} + \left(\frac{2}{3}F_c(\mathcal{R}) + \frac{N_c^2 - 1}{N_c^2}(1 - F_c(\mathcal{R})) \right) \hat{\rho}_{\mathbf{8}} \quad (28)$$

$$= \text{diag} \left(\frac{1}{3}F_c(\mathcal{R}) + \frac{1}{N_c^2}(1 - F_c(\mathcal{R})), \frac{2}{3(N_c^2 - 1)}F_c(\mathcal{R}) + \frac{1}{N_c^2}(1 - F_c(\mathcal{R})), \dots \right)_{\beta} \quad (29)$$

$$\equiv \text{diag}(\rho(R)_{\mathbf{1},\mathbf{1}}, \rho(R)_{\mathbf{8}_1,\mathbf{8}_1}, \dots)_{\beta}. \quad (30)$$

Again,

$$\begin{cases} \rho(\mathcal{R})_{\mathbf{8}_1,\mathbf{8}_1} = \rho(\mathcal{R})_{\mathbf{8}_2,\mathbf{8}_2} = \dots = \rho(\mathcal{R})_{\mathbf{8}_{N_c^2-1},\mathbf{8}_{N_c^2-1}} \\ \rho(\mathcal{R})_{\mathbf{a},\mathbf{b}} = 0 \quad (\text{for } \mathbf{a} \neq \mathbf{b}) \end{cases} \quad (31)$$

and the normalization condition

$$\text{Tr } \rho(\mathcal{R}) = \rho_{\mathbf{1}}(\mathcal{R}) + \rho_{\mathbf{8}}(\mathcal{R}) = 1, \quad (32)$$

$$\rho_{\mathbf{1}}(\mathcal{R}) \equiv \rho(\mathcal{R})_{\mathbf{1},\mathbf{1}}, \quad \rho_{\mathbf{8}}(\mathcal{R}) \equiv \sum_{i=1}^{N_c^2 - 1} \rho(\mathcal{R})_{\mathbf{8}_i,\mathbf{8}_i}. \quad (33)$$

are satisfied at any \mathcal{R} .

$F_c(\mathcal{R})$ can be reconstructed from $\rho_{\mathbf{1}}(\mathcal{R})$ or $\rho_{\mathbf{8}}(\mathcal{R})$ as

$$F_c(\mathcal{R}) = \frac{3}{N_c^2 - 3} (N_c^2 \rho_{\mathbf{1}}(\mathcal{R}) - 1). \quad (34)$$

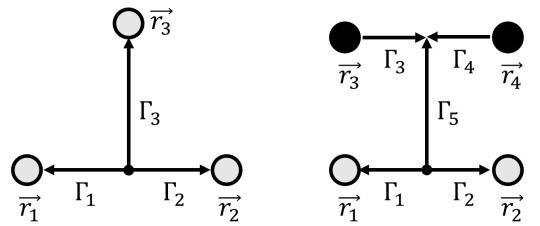


FIG. 1. The paths Γ_i that define the path-ordered products $U(\Gamma_i, t) \in \text{SU}(3)$ are shown for 3Q and 4Q cases.

C. Lattice QCD formalism

For the 3Q case, we locate static three quarks at $\mathcal{R} = \{\vec{r}_1, \vec{r}_2, \vec{r}_3\}$ in a xy plane, and define paths that stem from a junction point to \vec{r}_i ($i = 1, 2, 3$) as depicted in the left panel in Fig. 1. With the path-ordered products

$U(\Gamma_i, t) \in \text{SU}(3)$ at the Euclidean time t defined as

$$U(\Gamma_i, t) \equiv P \exp \left\{ ig \int_{\Gamma_i} A_\mu dx_\mu \right\}, \quad (35)$$

we define 3Q operator $Q_{c_1 c_2 c_3}^{3\text{Q}}(\mathcal{R}, t)$ as

$$Q_{c_1 c_2 c_3}^{3\text{Q}}(\mathcal{R}, t) \equiv \varepsilon^{abc} U_{c_1 a}(\Gamma_1, t) U_{c_2 b}(\Gamma_2, t) U_{c_3 c}(\Gamma_3, t), \quad (36)$$

$$Q_{c_1 c_2 c_3}^{3\text{Q}}(\mathcal{R}, t)^\dagger \equiv \varepsilon^{abc} U_{a c_1}^\dagger(\Gamma_1, t) U_{b c_2}^\dagger(\Gamma_2, t) U_{c c_3}^\dagger(\Gamma_3, t). \quad (37)$$

Here, the subscripts denote the color indices, and subscripts that appear twice are to be contracted. We can construct the correlator $C^{3\text{Q}}(T, \mathcal{R})$ for a static 3Q system as

$$C^{3\text{Q}}(\mathcal{R}, T) = Q_{c_1' c_2' c_3'}^{3\text{Q}}(\mathcal{R}, T)^\dagger Q_{c_1 c_2 c_3}^{3\text{Q}}(\mathcal{R}, 0) \times U_4(\vec{r}_1, T)_{c_1' c_1} U_4(\vec{r}_2, T)_{c_2' c_2} U_4(\vec{r}_3, T)_{c_3' c_3}. \quad (38)$$

$U_4(\vec{r}, T)$ is the path-ordered product in the temporal direction explicitly written as

$$U_4(\vec{r}, T) = P \exp \left\{ ig \int_{(\vec{r}, 0)}^{(\vec{r}, T)} A_4 dx_4 \right\}. \quad (39)$$

When we measure the color of Q_i , we replace the temporal part, $U_4(\vec{r}_i, T)$, in $C^{3\text{Q}}(\mathcal{R}, T)$ with

$$\begin{aligned} \tilde{U}_4(\vec{r}_i; T)_{ab, c'c} &\equiv P \exp \left\{ ig \int_{(\vec{r}_i, 0)}^{(\vec{r}_i, T/2)} A_4 dx_4 \right\}_{c'a} \\ &\times P \exp \left\{ ig \int_{(\vec{r}_i, T/2)}^{(\vec{r}_i, T)} A_4 dx_4 \right\}_{bc}, \end{aligned} \quad (40)$$

in which Q_i 's color is measured at the temporal point $t = T/2$ by inserting a quark operator $\hat{Q}_i^{\dagger a}(\vec{r}_i) \hat{Q}_i^b(\vec{r}_i)$ at $t = T/2$ plane. For example, when we measure the $Q_1 Q_2$ color correlation, we replace $U_4(\vec{r}_1, T)_{c_1' c_1}$ and $U_4(\vec{r}_2, T)_{c_2' c_2}$ in $C^{3\text{Q}}(\mathcal{R}, t)$ with $\tilde{U}_4(\vec{r}_1; T)_{ac, c_1' c_1}$ and $\tilde{U}_4(\vec{r}_2; T)_{bd, c_2' c_2}$, and define

$$\begin{aligned} \tilde{C}_{ab, cd}^{3\text{Q}}(\mathcal{R}, T) &\equiv Q_{c_1' c_2' c_3'}^{3\text{Q}}(\mathcal{R}, T)^\dagger Q_{c_1 c_2 c_3}^{3\text{Q}}(\mathcal{R}, 0) \\ &\times \tilde{U}_4(\vec{r}_1, T)_{ac, c_1' c_1} \tilde{U}_4(\vec{r}_2, T)_{bd, c_2' c_2} U_4(\vec{r}_3, T)_{c_3' c_3}. \end{aligned} \quad (41)$$

For the 4Q case, we locate static quarks and antiquarks at $\mathcal{R} = \{\vec{r}_1, \vec{r}_2, \vec{r}_3, \vec{r}_4\}$ in a xy plane, and define paths that stem from a junction to \vec{r}_i or to another junction as Γ_i ($i = 1 \sim 5$) as depicted in the right panel in Fig. 1. With the path-ordered products $U(\Gamma_i, t)$, we define 4Q operator $Q_{c_1 c_2, c_3 c_4}^{4\text{Q}}(\mathcal{R}, t)$ as

$$\begin{aligned} Q_{c_1 c_2, c_3 c_4}^{4\text{Q}}(\mathcal{R}, t) &\equiv \varepsilon^{abc} \varepsilon^{a'b'c'} U_{c_1 a}(\Gamma_1, t) U_{c_2 b}(\Gamma_2, t) \\ &\times U_{a'c_3}(\Gamma_3, t) U_{b'c_4}(\Gamma_4, t) U_{c'c}(\Gamma_5, t). \end{aligned} \quad (42)$$

We construct the correlator $C^{4\text{Q}}(T, \mathcal{R})$ for a static 4Q system as

$$\begin{aligned} C^{4\text{Q}}(\mathcal{R}, T) &= Q_{c_1' c_2' c_3' c_4'}^{4\text{Q}}(\mathcal{R}, T)^\dagger Q_{c_1 c_2, c_3 c_4}^{4\text{Q}}(\mathcal{R}, 0) \\ &\times U_4(\vec{r}_1, T)_{c_1' c_1} U_4(\vec{r}_2, T)_{c_2' c_2} U_4(\vec{r}_3, T)_{c_3' c_3} U_4(\vec{r}_4, T)_{c_4' c_4}^{(43)} \end{aligned}$$

As the 3Q case, replacing two of the temporal link variables in $C^{4\text{Q}}(\mathcal{R}, T)$ with $\tilde{U}_4(\vec{r}_i; T)_{ab, c'c}$ or $\tilde{U}_4(\vec{r}_i; T)_{ab, c'c}^\dagger$, we can measure the color structure of internal two (anti)quarks and construct $\tilde{C}_{ab, cd}^{4\text{Q}}(\mathcal{R}, T)$, from which we compute the two-body color density matrix $\rho(\mathcal{R})$ for 4Q systems.

When $\tilde{C}_{ab, cd}^{N\text{Q}}(\mathcal{R}, T)$ couples only to the ground state, $\langle \tilde{C}_{ab, cd}^{N\text{Q}}(\mathcal{R}, T) \rangle$ is then expressed as

$$\begin{aligned} &\langle \tilde{C}_{ab, cd}^{N\text{Q}}(\mathcal{R}, T) \rangle \\ &= A \langle NQ | e^{-\frac{1}{2} \hat{H} T} \hat{Q}_i^{\dagger a}(\vec{r}_i) \hat{Q}_j^{\dagger b}(\vec{r}_j) \hat{Q}_i^c(\vec{r}_i) \hat{Q}_j^d(\vec{r}_j) e^{-\frac{1}{2} \hat{H} T} | NQ \rangle \\ &= A e^{-E_0 T} \langle NQ | \hat{Q}_i^{\dagger a}(\vec{r}_i) \hat{Q}_j^{\dagger b}(\vec{r}_j) \hat{Q}_i^c(\vec{r}_i) \hat{Q}_j^d(\vec{r}_j) | NQ \rangle \\ &= B e^{-E_0 T} \int \mathcal{D}Q' \mathcal{D}G \times \\ &\quad \langle NQ | Q_i^a(\vec{r}_i) Q_j^b(\vec{r}_j) Q' G \rangle \langle Q_i^c(\vec{r}_i) Q_j^d(\vec{r}_j) Q' G | NQ \rangle \\ &= B e^{-E_0 T} \rho(\mathcal{R})_{ab, cd}, \end{aligned} \quad (44)$$

where E_0 is the ground state energy for the $N\text{Q}$ system. Q' and G again denote spectator quarks' and gluon's d.o.f. Normalizing $\langle \tilde{C}_{ab, cd}^{N\text{Q}}(\mathcal{R}, T) \rangle$ so that $\text{Tr} \langle \tilde{C}_{ab, cd}^{N\text{Q}}(\mathcal{R}, T) \rangle = \sum_{ab} \langle \tilde{C}_{ab, ab}^{N\text{Q}}(\mathcal{R}, T) \rangle = 1$, we finally obtain the two-body color density matrix $\rho(\mathcal{R})$ for the ground state $N\text{Q}$ state whose trace is unity ($\text{Tr} \rho(\mathcal{R}) = 1$).

D. Lattice QCD parameters

We perform quenched calculations of reduced density matrices of static quark pairs in multiquark (3Q, 4Q) systems adopting the standard Wilson gauge action. The gauge configurations are generated on the spatial volume of $V = 32^3$ with the gauge couplings $\beta = 5.8$, which corresponds to $V = 4.5^3$ [fm 3]. The temporal extent is $N_t = 32$. All the gauge configurations are gauge-fixed with the Coulomb gauge condition. While finite volume effects would still remain for $V = 4.5^3$ [fm 3] [10], a detailed study taking care of such systematic errors is beyond the scope of the present paper, in which the color structure of multiquark systems is clarified for the first time.

III. LATTICE QCD RESULTS (3Q)

A. spatial configuration

We locate three quarks at $(+d, 0, 0)$, $(-d, 0, 0)$, $(0, +h, 0)$ with integers d and h in a xy plane on the lat-

tice as seen in Fig. 2. When the color correlation between Q_1 and Q_2 (Q_1 and Q_3) is measured, it is an on-axis (off-axis) correlation. We adopt $1 \leq d \leq 4$ and $1 \leq h \leq 8$ for sets of (d, h) , totally 32 different spatial configurations.

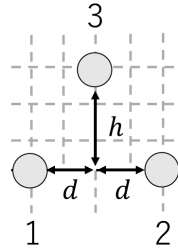


FIG. 2. Three quarks are located at $(+d, 0, 0)$, $(-d, 0, 0)$, $(0, +h, 0)$ with integers d and h on the lattice. When the correlation between 1- and 2-quarks (1- and 3-quarks) is measured, it is on-axis (off-axis) correlation.

B. Functional form of the ansatz

In the previous studies of $Q\bar{Q}$ systems, all the physical quantities were discussed based on the interquark distance R . It was actually found that the “initial” quarks’ color is screened by the in-between gluon flux tube, then the interquark distance R , which just coincides with the in-between flux tube length, is suitable for the analysis. In the analysis of 3Q systems, taking into account that color screening or color absorption occurs inside a flux tube, we evaluate physical quantities based on the length L of the flux-tube path between two quarks of which we investigate the color structure. As for the flux-tube shape, we consider the Y-type confining flux tube appearing in the ground-state 3Q systems [3, 7].

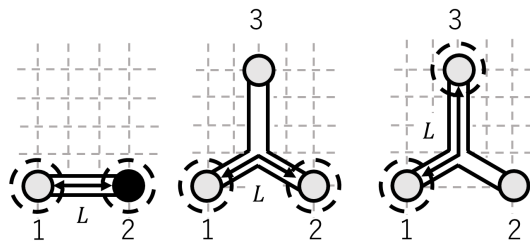


FIG. 3. Shematic pictures which express the definition of L in $Q\bar{Q}$ and 3Q systems. Two (anti)quarks of which we measure the color correlation are enclosed in dotted circles.

Figure 3 shows schematic pictures of L . Two (anti)quarks of which we measure the color correlation are enclosed in dotted circles. In the $Q\bar{Q}$ case (left panel), the flux-tube path length L coincides with the interquark distance R . In 3Q systems (middle and right panels), where there appears a Y-type flux tube that has a junction, the flux-tube path length L is defined as the shortest

distance along the flux tube between two quarks, Q_i and Q_j ($i \neq j$), under consideration.

C. Antitriplet and sextet components

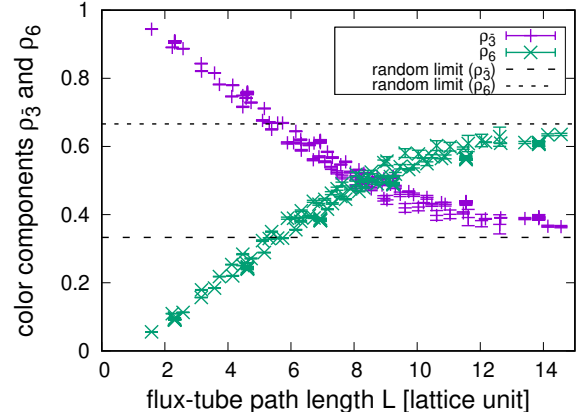


FIG. 4. Antitriplet and sextet components (ρ_3 and ρ_6) for 3Q systems plotted as a function of L . The dashed and dotted lines indicate the values $\frac{3}{9}$ and $\frac{6}{9}$ for ρ_3 and ρ_6 in the random-limit color configuration, respectively.

Figure 4 shows the L dependence of the antitriplet and sextet components ρ_3 and ρ_6 that a QQ pair possesses in the 3Q systems. These components are measured in both of Q_1Q_2 and Q_1Q_3 pairs in Fig. 2, and they are simultaneously plotted with the same symbols in the figure. One can find that a QQ pair in the 3Q system forms a purely *color antitriplet* configuration at $L \rightarrow 0$, and the ratio $\rho_3 : \rho_6$ approaches $3 : 6$ of the random color configuration as L increases. Although the color components are measured for various 3Q spatial configurations (various d and h), ρ_3 and ρ_6 seem to depend solely on L and are almost single-valued functions of L .

From these observations, we can expect that *the QQ color configuration in 3Q systems with $\mathcal{R} \rightarrow 0$ coincides with the MC color configuration ($[Q_1Q_2]Q_3$), and that the QQ color configuration is randomized when the 3Q system size is enlarged*. It indicates that the ansatz (Eq. (13)) works well for 3Q systems.

As seen in the next subsection, ρ_3 and ρ_6 exponentially damp towards the random limit as a function of L , which implies that the quarks’ color is screened inside the gluon flux tube connecting two quarks under investigation. The exponential damping indicates that in-between flux tube formation is expressed by the color leak from color sources to a gluon flux tube, and can be quantified by the residual rate $F_3(\mathcal{R})$ of the MC color configuration defined in the ansatz as given in Eq. (13).

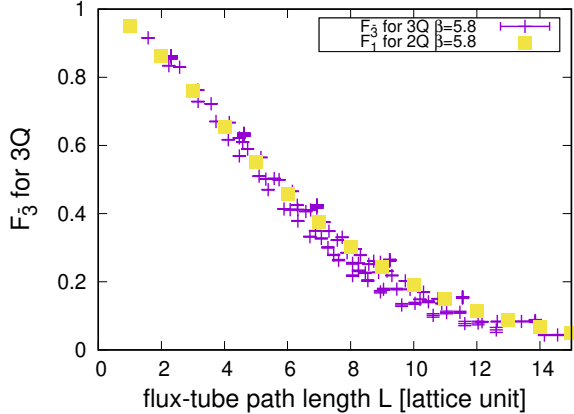


FIG. 5. $F_{\bar{3}}^{3Q}(\mathcal{R})$ is plotted as a function of L . The square symbols denote $F_1^{2Q}(\mathcal{R})$ obtained in a $Q\bar{Q}$ system.

D. L dependence of $F_1(\mathcal{R})$

In Fig. 5, the residual rate $F_{\bar{3}}^{3Q}(\mathcal{R})$ obtained in 3Q systems is plotted as a function of L . The residual rate $F_1^{2Q}(\mathcal{R})$ obtained in $Q\bar{Q}$ systems denoted by square symbols is also plotted as a function of $L = R$. $F_1^{2Q}(\mathcal{R})$ used here are the same data as shown in Ref. [10]. The positions \mathcal{R} of the quark and antiquark were set to $\mathcal{R} = \{\vec{r}_1, \vec{r}_2\} = \{(0, 0, 0), (R, 0, 0)\}$ in the calculation. As a remarkable fact, one can find a good coincidence between these two functions $F_{\bar{3}}^{3Q}(\mathcal{R})$ and $F_1^{2Q}(\mathcal{R})$. It implies that the color initially associated with quarks is screened “inside” the flux tube, and the screening strength enlarges as the flux tube grows showing the same L dependence in both of $Q\bar{Q}$ and 3Q systems.

IV. LATTICE QCD RESULTS (4Q)

A. spatial configuration

We put quarks and antiquarks at $(+d, 0, 0)$, $(-d, 0, 0)$, $(-d, h, 0)$ and $(+d, h, 0)$ with integers d and h in the case of planar spatial configurations, and quarks and antiquarks are located at $(+d, 0, 0)$, $(-d, 0, 0)$, $(0, h, -d)$ and $(0, h, +d)$ in the case of twisted spatial configurations, as seen in Fig. 6. We adopt $1 \leq d \leq 4$ and $1 \leq h \leq 8$ for sets of (d, h) , totally 32 different spatial configurations.

B. Energy spectrum

The most prominent difference in color structure between twisted and planar systems can be seen when large d is adopted. In the case of a planar spatial configuration, flux-tube rearrangement (flip-flop) occurs as shown in Fig. 7, and both of “connected 4Q configuration” and “disconnected 4Q configuration” appear depending on

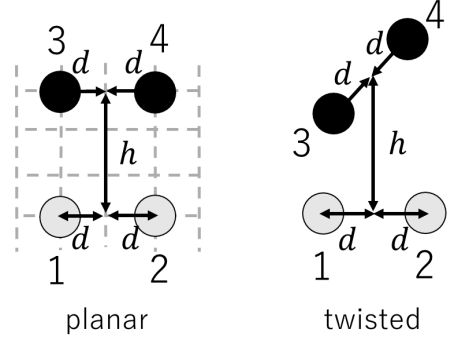


FIG. 6. Quarks and antiquarks are located at $(+d, 0, 0)$, $(-d, 0, 0)$, $(-d, h, 0)$ and $(+d, h, 0)$ in the case of planar spatial configurations. Quarks and antiquarks are located at $(+d, 0, 0)$, $(-d, 0, 0)$, $(0, h, -d)$ and $(0, h, +d)$ in the case of twisted spatial configurations.

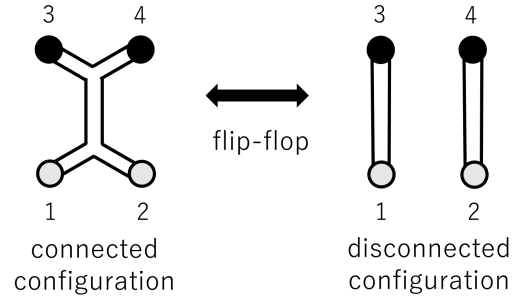


FIG. 7. In connected 4Q configurations (left), all the quarks are connected with a double-Y type flux tube [4]. In disconnected 4Q configurations (right), quark and antiquark are connected with a straight flux tube, and the system consists of two “mesons” (two $Q\bar{Q}$ ’s). These two configurations transform into one another through the rearrangement of flux tubes called a flip-flop.

the parameters, h and d . On the other hand, in the case of a twisted spatial 4Q configuration, the “connected 4Q configuration” shown in the left panel in Fig. 7 is always energetically favored [8], and no flip-flop occurs.

In Fig. 8, the data with errorbars labeled “E ($d = i$) [La]” show the energy spectra of twisted 4Q systems for each d plotted as a function of h . Solid lines labeled “E ($d = i$) [Th]” show theoretical expectation values for connected 4Q configurations that are obtained assuming a Coulomb plus double-Y type linear confinement potential. Note that the flux-tube profile takes the X-type configuration with large d and small h [4, 8], which is also included in the computation of the theoretical values. One can find that all the lattice data lie on “E ($d = i$) [Th]” curves and confirm that no flip-flop occurs in twisted 4Q systems.

In Fig. 9, the data with errorbars labeled “E ($d = i$) [La]” represent the energy spectra of planar 4Q systems for each d plotted as a function of h . Solid lines la-

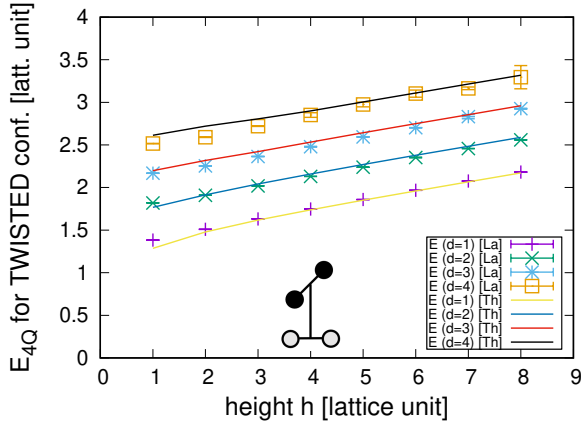


FIG. 8. The data with errorbars labeled “E ($d = i$) [La]” show the energy spectra of twisted 4Q configurations for each d plotted as a function of h . Solid lines labeled “E ($d = i$) [Th]” show theoretical expectation values for “connected” 4Q configurations obtained assuming a Coulomb plus double-Y type (X-type) linear confinement potential.

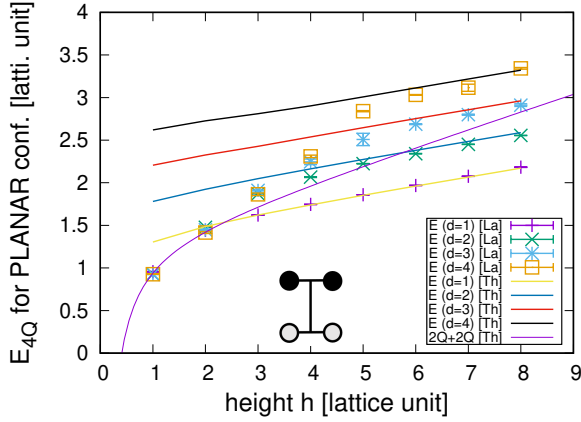


FIG. 9. The data with errorbars labeled “E ($d = i$) [La]” show the energy spectra of planar 4Q configurations for each d plotted as a function of h . Solid lines labeled “E ($d = i$) [Th]” show theoretical expectation values for “connected” 4Q configurations obtained assuming a Coulomb plus double-Y type (X-type) linear confinement potential. Solid lines labeled “2Q+2Q” show theoretical expectation values for “disconnected” 4Q configurations assuming that the system is split into “two mesons” as a result of flip-flop.

beled “E ($d = i$) [Th]” show theoretical expectation values for connected 4Q configurations assuming a Coulomb plus double-Y type (X-type) linear confinement potential. The solid line labeled “2Q+2Q[Th]” shows the theoretical expectation value for disconnected 4Q configurations obtained assuming that the system is split into “two mesons” as a result of flip-flop. In this case, 4Q energy data approach or lie on a “2Q+2Q[Th]” curve at small h . These observations are consistent with the previous work [8].

C. Functional form of the ansatz

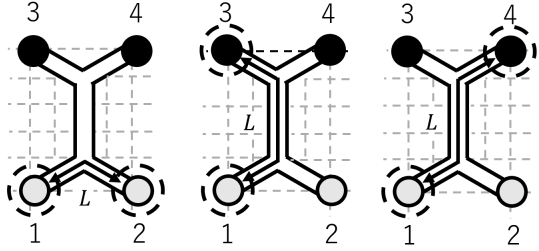


FIG. 10. Schematic pictures which express the definition of L for 4Q systems. Two quarks (antiquarks) of which we measure the color correlation are enclosed in dotted circles.

In the 4Q case, we also evaluate physical quantities based on the flux-tube path length L between two quarks under consideration. As for the flux-tube shape, we assume a double-Y type (X-type) confining flux tube appearing in ground-state tetraquark systems [4, 8]. Figure 10 shows schematic pictures of L for two quarks (antiquarks) enclosed in dotted circles.

Note that planar 4Q systems forming a disconnected configuration ($Q\bar{Q}+Q\bar{Q}$ state) do not have such double-Y type flux tubes, but they have two separated flux tubes (the right panel in Fig. 7), where L can not be defined as a function of d and h , hence the color correlation of quark pairs would not exhibit proper L dependence because of flip-flop.

D. $\rho_{\bar{3}}$ and ρ_1 in twisted 4Q configurations

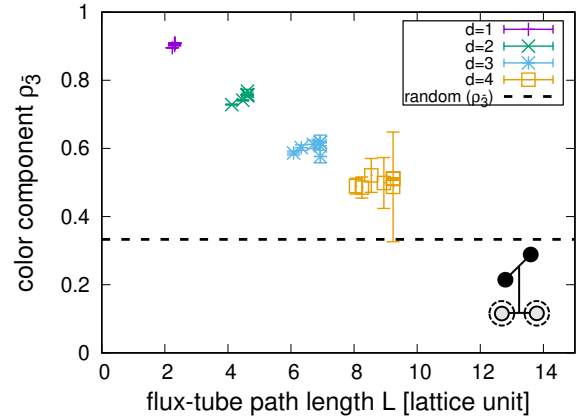


FIG. 11. Antitriplet components ($\rho_{\bar{3}}$) for twisted 4Q systems plotted as a function of L . The dashed line indicates the random-limit value, $\rho_{\bar{3}} = 3/9$.

Figure 11 shows the L dependence of the antitriplet components ($\rho_{\bar{3}}$) in the Q_1Q_2 pair (the left panel of Fig. 10) in twisted 4Q spatial configurations, and Fig. 12

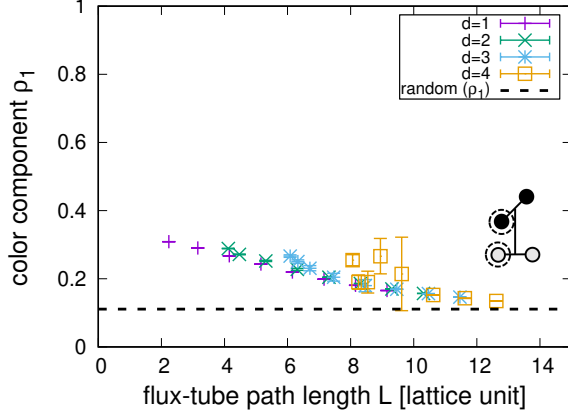


FIG. 12. Singlet components (ρ_1) for twisted 4Q systems plotted as a function of L . The dashed line indicates the random-limit value, $\rho_1 = 1/9$.

shows the singlet components (ρ_1) in the $Q_1\bar{Q}_3$ pair (the middle panel of Fig. 10). The dashed line in both figures indicates $3/9$ and $1/9$, which are the random-limit values of ρ_3 and ρ_1 , respectively. Note that the density matrix for the $Q_1\bar{Q}_4$ pair (the right panel of Fig. 10) coincides with that for $Q_1\bar{Q}_3$ due to the rotational and reflection symmetry on the lattice.

In Figs. 11 and 12, we can see that ρ_3 and ρ_1 can be expressed by a single function of L . In the case of ρ_3 for the QQ pair, it starts from $\rho_3 = 1$ at $L \sim 0$ and gradually approaches $\rho_3 = 3/9$. $\rho_3 = 1$ implies that QQ pair in the ground-state 4Q system forms a purely color triplet state, and the QQ 's color configuration can be expressed purely by $\hat{\rho}_3$ at $L \sim 0$. ρ_3 approaching the random limit value $3/9$ shows that a QQ pair's color configuration is randomized at large L region. On the other hand, ρ_1 for the $Q\bar{Q}$ pair starts from $\rho_1 = 1/3$ at $L \sim 0$ and gradually approaches the random-limit value, $\rho_1 = 1/9$, at large L . $\rho_1 = 1/3$ implies that $Q\bar{Q}$ pair's color configuration in the ground-state 4Q system is a combination of a color singlet and color octet configurations with the ratio $\rho_1 : \rho_8 = 1 : 2$, which means that the color state at $L \sim 0$ can be expressed by $\hat{\rho}^{\text{combi}} = \frac{1}{3}\hat{\rho}_1 + \frac{2}{3}\hat{\rho}_8$ defined in Eq. (24) for the $Q\bar{Q}$ pair in the MC color configuration. ρ_1 approaching $1/9$ shows that $Q\bar{Q}$ pair's color configuration is again randomized at large L region.

From these observations, we can expect that the quark color configuration for small 4Q systems ($\mathcal{R} \rightarrow 0$) coincides with the MC color configuration ($[Q_1Q_2][\bar{Q}_3\bar{Q}_4]$), and that the quark color configuration is randomized when the 4Q system size is enlarged as expected. Namely, the ansatz (Eqs. (13) and (25)) works well also for twisted 4Q systems.

In Figs. 13 and 14, the residual rates of ρ_3 and $\hat{\rho}^{\text{combi}}$, $F_3^{4Q}(\mathcal{R})$ and $F_c^{4Q}(\mathcal{R})$, are plotted as a function of L . In both figures, the square symbols labeled “ F_1^{2Q} ” represent $F_1^{2Q}(\mathcal{R})$ obtained in 2Q ($Q\bar{Q}$) systems. Figure 13 shows good agreement in the L dependence between $F_3^{4Q}(\mathcal{R})$

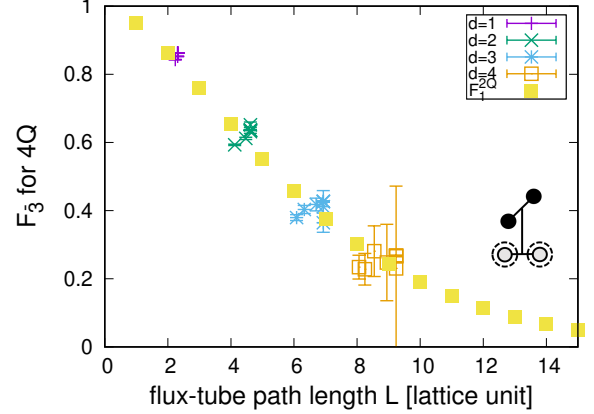


FIG. 13. The residual rate $F_3^{4Q}(\mathcal{R})$ in Eq. (13) for twisted 4Q systems plotted as a function of L . The data labeled “ F_1^{2Q} ” here represents $F_1^{2Q}(\mathcal{R})$ obtained in 2Q ($Q\bar{Q}$) systems.

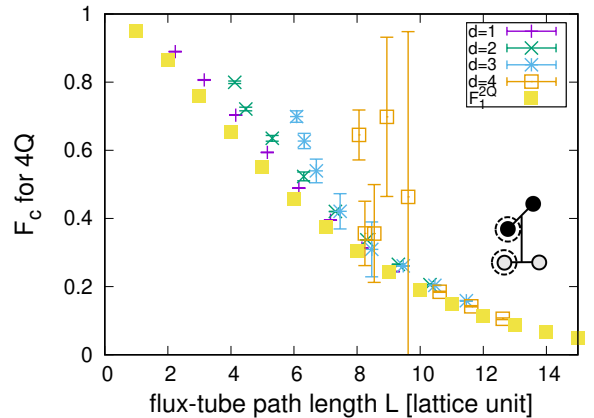


FIG. 14. The residual rate $F_c^{4Q}(\mathcal{R})$ in Eq. (25) for twisted 4Q systems plotted as a function of L . The data labeled “ F_1^{2Q} ” here represents $F_1^{2Q}(\mathcal{R})$ obtained in 2Q ($Q\bar{Q}$) systems.

and $F_1^{2Q}(\mathcal{R})$, which indicates that the color screening occurs inside a gluon flux tube connecting two quarks (QQ) also for 4Q cases, and its screening effect enlarges along the flux-tube path. While $F_c^{4Q}(\mathcal{R})$ globally coincides with $F_1^{2Q}(\mathcal{R})$ as seen in Fig. 14, one can find some deviation from $F_1^{2Q}(\mathcal{R})$ line especially for larger d and smaller h . One possible reason for the deviation might be the flux-tube profile. When large d and small h are employed, the flux-tube profile approaches the X-type configuration [4, 8]. In this X-type flux configuration, the number of junctions is one, and angles between tubes are no longer $\frac{2}{3}\pi$. It is in contrast to the double-Y type configuration, in which there appear two junctions on the flux-tube path between Q and \bar{Q} , and angles between tubes all remain $\frac{2}{3}\pi$.

E. $\rho_{\bar{3}}$, $\rho_1^{\{1,3\}}$ and $\rho_1^{\{1,4\}}$ in planar 4Q configurations

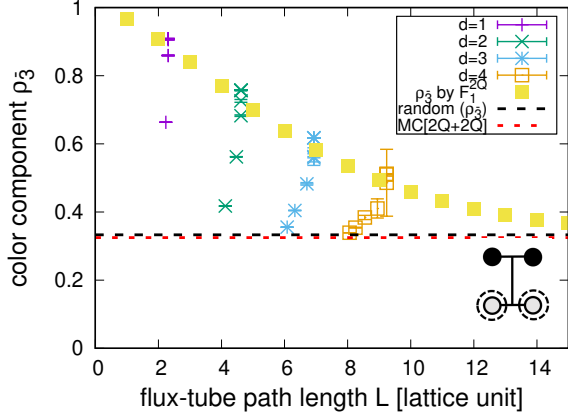


FIG. 15. Antitriplet components ($\rho_{\bar{3}}$) for planar 4Q systems plotted as a function of L . The black dashed line indicates $3/9$ representing the random limit value of $\rho_{\bar{3}}$. The red dotted line labeled “MC[2Q+2Q]” shows $3/9$, which is the value of $\rho_{\bar{3}}$ expected when a system forms a “disconnected 4Q configuration”. The data labeled “ $\rho_{\bar{3}}$ by F_1^{2Q} ” here represents the reconstructed values of $\rho_{\bar{3}}$ when $F_1^{2Q}(\mathcal{R})$ for $Q\bar{Q}$ systems is inserted into $F_{\bar{3}}(\mathcal{R})$ in Eq. (13).

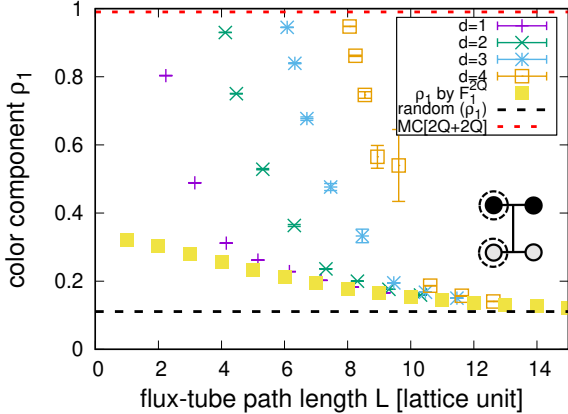


FIG. 16. Singlet components ($\rho_1^{\{1,3\}}$) for planar 4Q systems plotted as a function of L . The black dashed line indicates $1/9$ representing the random limit value of ρ_1 . The red dotted line labeled “MC[2Q+2Q]” shows 1 , which is the value of $\rho_1^{\{1,3\}}$ expected when a system forms a “disconnected 4Q configuration” and each $Q\bar{Q}$ pair forms the MC configuration (pure color singlet configuration). The data labeled “ ρ_1 by F_1^{2Q} ” here represents the reconstructed values of ρ_1 when $F_1^{2Q}(\mathcal{R})$ for $Q\bar{Q}$ systems is inserted into $F_c(\mathcal{R})$ in Eq. (25).

Figure 15 shows the antitriplet components ($\rho_{\bar{3}}$) for a $Q_1\bar{Q}_2$ pair in planar 4Q systems plotted as a function of the flux-tube path length L . The black dashed line indicates the random limit value $3/9$ of $\rho_{\bar{3}}$. The red dotted line labeled “MC[2Q+2Q]” shows $\rho_{\bar{3}} = 3/9$, the value expected in the MC limit of a “disconnected 4Q con-

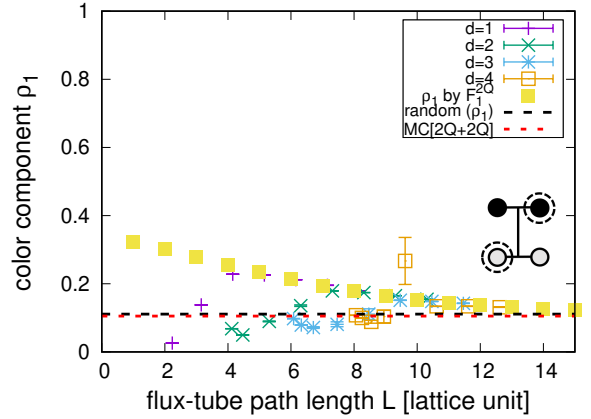


FIG. 17. Singlet components ($\rho_1^{\{1,4\}}$) for planar 4Q systems plotted as a function of L . The black dashed line indicates $1/9$ representing the random limit value of ρ_1 . The red dotted line labeled “MC[2Q+2Q]” shows $1/9$, which is the value of $\rho_1^{\{1,4\}}$ expected when a system forms a “disconnected 4Q configuration”. The data labeled “ ρ_1 by F_1^{2Q} ” here represents the reconstructed values of ρ_1 when $F_1^{2Q}(\mathcal{R})$ for $Q\bar{Q}$ systems is inserted into $F_c(\mathcal{R})$ in Eq. (25).

figuration”. This value coincides with the random-limit value ($\rho_{\bar{3}} = 3/9$), since in disconnected 4Q configurations, Q_1 and Q_2 belong to different color singlet $Q\bar{Q}$ clusters, and have no color correlation. The data labeled “ $\rho_{\bar{3}}$ by F_1^{2Q} ” here represent the reconstructed values of $\rho_{\bar{3}}$ when $F_1^{2Q}(\mathcal{R})$ for $Q\bar{Q}$ systems is inserted into $F_{\bar{3}}(\mathcal{R})$ in Eq. (13).

Figure 16 shows the singlet components ($\rho_1^{\{1,3\}}$) measured in a $Q_1\bar{Q}_3$ pair in planar 4Q systems plotted as a function of the flux-tube path length L . The black dashed line indicates the random limit value, $\rho_1^{\{1,3\}} = 1/9$. The red dotted line labeled “MC[2Q+2Q]” shows $\rho_1^{\{1,3\}} = 1/9$. The data labeled “ ρ_1 by F_1^{2Q} ” here represents the reconstructed values of ρ_1 when $F_1^{2Q}(\mathcal{R})$ for $Q\bar{Q}$ systems is inserted into $F_c(\mathcal{R})$ in Eq. (25).

Figure 17 shows the singlet components ($\rho_1^{\{1,4\}}$) measured in a $Q_1\bar{Q}_4$ pair in planar 4Q systems plotted as a function of the flux-tube path length L . The black dashed line indicates the random limit value, $\rho_1^{\{1,4\}} = 1/9$. The red dotted line labeled “MC[2Q+2Q]” shows $\rho_1^{\{1,4\}} = 1/9$, the value expected in the MC limit of a disconnected 4Q configuration. In disconnected 4Q configurations, Q_1 and \bar{Q}_4 belong to different color singlet $Q\bar{Q}$ clusters, and have no color correlation leading to $\rho_1 \sim 1/9$. The data labeled “ ρ_1 by F_1^{2Q} ” represents the reconstructed values of ρ_1 when $F_1^{2Q}(\mathcal{R})$ for $Q\bar{Q}$ systems is inserted into $F_c(\mathcal{R})$ in Eq. (25).

In planar 4Q systems, systems would form a connected

4Q configuration at large h . With a decrease of h , the energy of a “two-meson state” comes down lower than that of genuine connected 4Q states, and the system will undergo flip-flop and form a disconnected 4Q state at small h . In such disconnected 4Q cases, if we measure $\rho_{\bar{3}}$ or $\rho_1^{\{1,4\}}$ in 4Q systems, it would take the random-limit value $\rho_{\bar{3}} = 3/9$ ($\rho_1^{\{1,4\}} = 1/9$), since Q_1 and $Q_2(\bar{Q}_4)$ under investigation belong to different color singlet clusters and have no color correlation. Even in connected 4Q systems, $\rho_{\bar{3}}$ and $\rho_1^{\{1,4\}}$ also approach the random limit values ($\rho_{\bar{3}} = 3/9$, $\rho_1^{\{1,4\}} = 1/9$) in the large L limit due to the color screening inside a flux tube, but the L dependence of $\rho_{\bar{3}}$ and $\rho_1^{\{1,4\}}$ in this case would be on the expected curve as shown later, and we can discriminate these behaviors. When we measure $Q_1\bar{Q}_3$ color correlation in disconnected 4Q systems with small h , $\rho_1^{\{1,3\}}$ would be 1, since Q_1 and \bar{Q}_3 under investigation belong to the same color singlet cluster and have maximal color correlation.

The lattice data $\rho_{\bar{3}}$ in Fig. 15 for small h lie around $\rho_{\bar{3}} = 3/9$ (random limit value), which indicates that there is no color correlation between two quarks (Q_1Q_2) under investigation and systems are just forming disconnected 4Q configurations. As h increases, the data approach the values reconstructed from $F_1^{2Q}(\mathcal{R})$ for $Q\bar{Q}$ systems (filled square symbols in the figures), which shows that the systems are genuine connected 4Q states for large h , and $\rho_{\bar{3}}$ shows the proper L dependence that is expected for the connected 4Q case.

The lattice data $\rho_1^{\{1,3\}}$ in Fig. 16 for small h lie around $\rho_1^{\{1,3\}} = 1$, which indicates that $Q_1\bar{Q}_3$ under investigation are forming a genuine color-singlet pair and shows that systems are divided into two-meson clusters in a disconnected 4Q state. As h increases, the data approach the values reconstructed from $F_1^{2Q}(\mathcal{R})$ for $Q\bar{Q}$ systems (filled square symbols in the figures), which again confirms that the systems are genuine connected 4Q states for large h .

The lattice data $\rho_1^{\{1,4\}}$ in Fig. 17 for small h lie around $\rho_1^{\{1,4\}} = 1/9$, which indicates that $Q_1\bar{Q}_4$ under investigation have no color correlation and belong to different color-singlet clusters, and that systems are 4Q disconnected states. As h increases, the data approach the values reconstructed from $F_1^{2Q}(\mathcal{R})$ for $Q\bar{Q}$ systems (filled square symbols in the figures), which repeatedly shows that the systems are genuine connected 4Q states for large h . In these analyses, the data for $d = 1$ and small h show slightly unexpected behaviors, which is considered to reflect possible remaining interactions between two-mesons.

Based on the analyses of 2Q, 3Q, and 4Q systems, we find the following.

- When a system size is small and no gluon flux tube is present, quarks form the “maximally correlated (MC)” color configuration, which is naively expected when we ignore gluon’s color.

- As a system size is enlarged and a long gluon flux tube grows, quarks’ color is screened inside the flux tube, and finally the quarks’ color configuration approaches the “random” color configuration, in which all the color components equally contribute, as a result of color screening.

- The color configuration of any quark pair can be represented by the color density operator

$$\hat{\rho}^{\text{ansatz}}(\mathcal{R}) = F_{\text{MC}}(\mathcal{R})\hat{\rho}^{\text{MC}} + (1 - F_{\text{MC}}(\mathcal{R}))\hat{\rho}^{\text{rand}}.$$

$\hat{\rho}^{\text{MC}}$ and $\hat{\rho}^{\text{rand}}$ correspond to the operators for the MC color configuration and the random configuration, respectively. $F_{\text{MC}}(\mathcal{R})$ is the residual rate of the MC color configuration, which is a monotonous function of a flux-tube path length L .

- The flux-tube path length L dependence of the residual rates of the MC color configurations ($F_1^{2Q}(\mathcal{R})$, $F_{\bar{3}}^{3Q}(\mathcal{R})$, $F_{\bar{3}}^{4Q}(\mathcal{R})$ and $F_c^{4Q}(\mathcal{R})$) all retain *universality*; the universal L dependence of the color screening effect along the flux-tube path.
- When two quarks in a pair under consideration belong to different color singlet clusters (mesons), they have no color correlation and their color configuration is expressed by the random color configuration, which can be useful to identify the internal structure of multiquark states.

V. ANALYSIS WITH ENTANGLEMENT ENTROPY

Entanglement entropy (EE) [10, 11, 13–19] defined by a reduced density matrix reflects and quantifies the correlation between the d.o.f. in the reduced density matrix and the traced-out d.o.f. in a full density matrix. Let us consider a system which is divided into subsystems A and B . Defining

$$\rho_A \equiv \text{Tr}_B (\rho_{\text{full}}),$$

a reduced density matrix obtained by tracing out the d.o.f. for the subsystem B , an entanglement entropy S^{EE} in the functional form of the von Neumann entropy is expressed as

$$S^{\text{EE}} = -\text{Tr}_A (\rho_A \log \rho_A) \equiv S^{\text{vN}}, \quad (45)$$

and EE in the form of the Renyi entropy of the order α can be expressed as

$$S^{\text{EE}} = \frac{1}{1 - \alpha} \log \text{Tr}_A (\rho_A^\alpha) \equiv S^{\text{Renyi} - \alpha}. \quad (46)$$

S^{EE} represents the correlation between subsystems A and B , and $S^{\text{EE}} \sim 0$ ($S^{\text{EE}} \gg 0$) holds when the correlation between A and B is weak (strong).

Quark color correlations can be also quantified from the viewpoint of an entanglement entropy (EE) [10, 11]. EE constructed from a reduced two-body color density matrix ρ , which is obtained by integrating out the d.o.f. other than a target quark pair, can quantify the color correlation between the quark pair and the “outside region”. The “outside region” here contains in-between gluon fields and all the spectator quarks, whose d.o.f. are all integrated out in the construction of the reduced two-body density matrix ρ . The situation is illustrated in Fig. 18. The quark pair of which we investigate the correlation belongs to the subsystem A , and the other d.o.f. including gluons and spectator quarks are all included in the subsystem B in the above example.

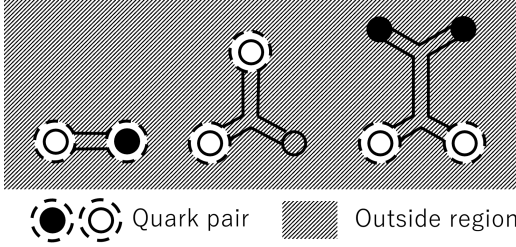


FIG. 18. Two quarks in a pair we investigate are enclosed in dotted circles. The “outside region” contains in-between gluon fields and spectator quarks, whose d.o.f. are all integrated out in the construction of the reduced two-body density matrix ρ .

In the 2Q ($Q\bar{Q}$) case, when no physical gluon flux tube is present in a system, the quark pair’s color does NOT leak into the “outside region”: the color flowing out from one (anti)quark is fully absorbed by the other (anti)quark, and the color d.o.f. of the quark pair decouples from the outside region. As a result, the color correlation between quarks of the pair is maximized, and the entanglement (color correlation) between the quark pair and “outside region” is zero, which leads to the minimal value of EE ($S \sim 0$). When long gluon flux tubes are formed in a system, quark pair’s color largely leak into the flux tube, “outside region”. This color screening in the flux tube weakens the interquark color correlation, and gives a strong entanglement between the quark pair and “outside region” providing a large value of EE ($S \gg 0$). The quark pair’s color configuration is randomized due to the screening by in-between gluons when a flux tube is formed between quarks.

In the case of 3Q (QQQ) and 4Q ($QQ\bar{Q}\bar{Q}$) cases, the color from a target quark pair can be absorbed also by the spectator quark(s), which produces a finite color correlation between the pair and the “outside region”, and it gives a finite EE ($S > 0$) even when no physical gluon flux tube is present. EE can quantify the internal color structure in this way, and we utilize an entanglement entropy to cast light on the internal color structure of multiquark systems.

In this study, we employ the second order Renyi entan-

glement entropy by taking $\alpha = 2$, which is simply given by the squared $\rho(\mathcal{R})$ as

$$S^{\text{Renyi-2}}(\mathcal{R}) = -\log \text{Tr}(\rho(\mathcal{R})^2). \quad (47)$$

A. EE for planar 4Q configurations

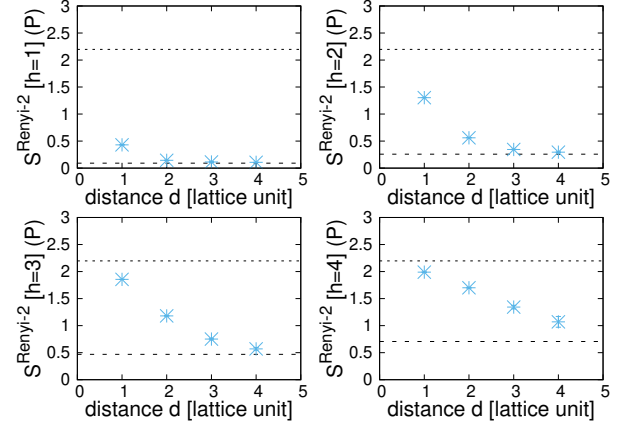


FIG. 19. $S^{\text{Renyi-2}}$ for planar 4Q configurations with $h = 1 \sim 4$, which are measured with Q_1 and \bar{Q}_3 , are plotted as a function of d . The upper line denotes $S^{\text{Renyi-2}} = \log(N_c^2)$, which holds when Q_1 and \bar{Q}_3 form a purely random-color state and have no color correlation. The lower line denotes $S^{\text{Renyi-2}}$ value when Q_1 and \bar{Q}_3 belong to the identical color-singlet cluster forming a meson state with the interquark distance $R = h$, which was separately measured with same parameters in a $Q\bar{Q}$ system.

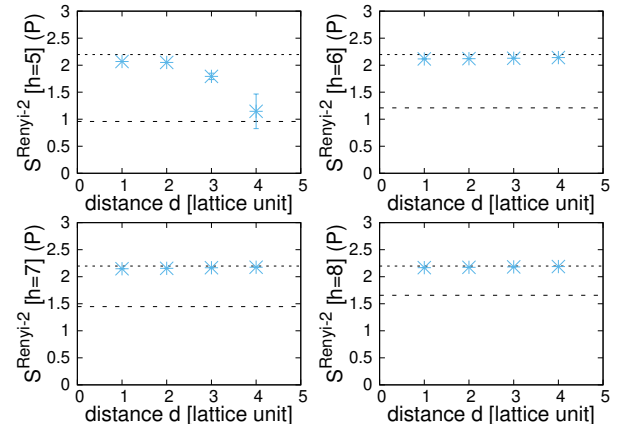


FIG. 20. $S^{\text{Renyi-2}}$ for planar 4Q configurations with $h = 5 \sim 8$, which are measured with Q_1 and \bar{Q}_3 , are plotted as a function of d . The upper line denotes $S^{\text{Renyi-2}} = \log(N_c^2)$, which holds when Q_1 and \bar{Q}_3 form a purely random-color state and have no color correlation. The lower line denotes $S^{\text{Renyi-2}}$ value when Q_1 and \bar{Q}_3 belong to the identical color-singlet cluster forming a meson state with the interquark distance $R = h$, which was separately measured with same parameters in a $Q\bar{Q}$ system.

In Figs. 19 and 20, $S^{\text{Renyi-2}}$ for planar 4Q configurations with $h = 1 \sim 8$, which are measured with Q_1 and \bar{Q}_3 , are plotted as a function of d . The upper line denotes the maximal value $S^{\text{Renyi-2}} = \log(N_c^2)$ for a $Q_1\bar{Q}_3$ pair forming a purely random-color state and having no color correlation. We again note that *no correlation* inside the target pair implies a *maximal correlation* between the pair and “outside region”. We also show the $S^{\text{Renyi-2}}$ value of an isolated $Q\bar{Q}$ system (a meson state) with the interquark distance $R = h$ by the lower line, which was separately calculated with the same parameters in a $Q\bar{Q}$ system.

In three panels for $h = 1 \sim 3$, S values are consistent with the two-meson state values denoted by the lower lines at large d region, $d > h$. It indicates that Q_1 and \bar{Q}_3 quarks with a large d and small h in the planar 4Q configuration belong to the same color singlet $Q_1\bar{Q}_3$ cluster, reflecting the fact that the four quarks are separated into two meson clusters forming a disconnected 4Q configuration as a result of flip-flop (the right panel in Fig. 7). In this case, the color from the $Q_1\bar{Q}_3$ pair is absorbed and screened only by in-between flux tube, and does not flow out from the $Q_1\bar{Q}_3$ cluster.

On the other hand, in the panels for $h = 6 \sim 8$ in Fig. 20, S lie on the upper line denoting the maximal value of S , which shows that $Q_1\bar{Q}_3$ pair’s color largely leaks into the “outside region”. It implies that there exist long flux tube connecting Q_1 and \bar{Q}_3 , and that the system would be a genuine connected 4Q state (the left panel in Fig. 7) in the large h region. In this connected 4Q case, the color of $Q_1\bar{Q}_3$ pair also flows into spectator quarks Q_2 and \bar{Q}_4 as well as in-between flux tube, which further enlarges S .

The 4Q states whose EE values lie between the two reference lines are considered to be in the transient stage of color rearrangement (flip-flop) process.

B. EE for twisted 4Q configurations

In Figs. 21 and 22, $S^{\text{Renyi-2}}$ for twisted 4Q configurations with $h = 1 \sim 8$, which are measured with Q_1 and \bar{Q}_3 , are plotted as a function of d . The dotted line denotes $S^{\text{Renyi-2}} = \log(N_c^2)$, the maximal value of EE. In stark contrast to the planar 4Q case, EE takes large values close to $\log(N_c^2)$ even with small h and d , and the large EE in these regions implies large color leak from a quark pair to the “outside region”. Taking into account that in-between flux tube has not grown well in these small-size regions, the quark pair’s color does not leak to in-between gluons but partially flows to other “spectator” quarks (Q_2 and \bar{Q}_4), which again verifies that four quarks are “connected” in terms of color in twisted 4Q systems.

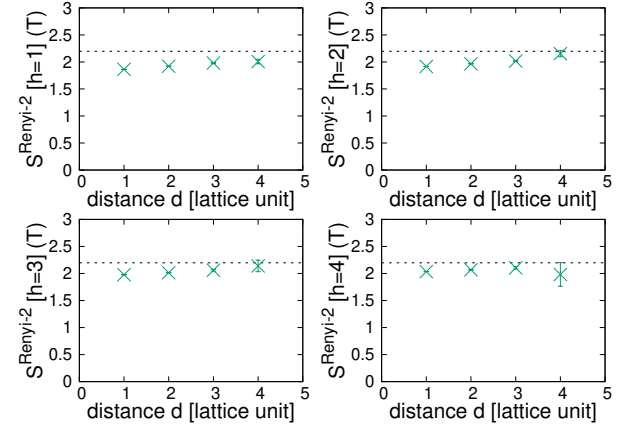


FIG. 21. $S^{\text{Renyi-2}}$ for twisted 4Q configurations with $h = 1 \sim 4$, which are measured with Q_1 and \bar{Q}_3 , are plotted as a function of d . The dotted line denotes $S^{\text{Renyi-2}} = \log(N_c^2)$, the maximum value of EE.

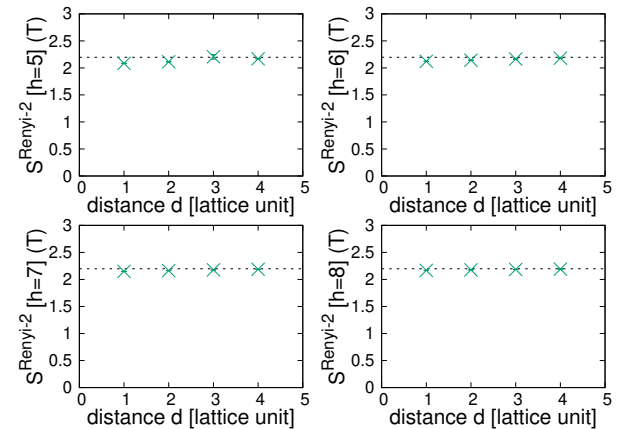


FIG. 22. $S^{\text{Renyi-2}}$ for twisted 4Q configurations with $h = 5 \sim 8$, which are measured with Q_1 and \bar{Q}_3 , are plotted as a function of d . The dotted line denotes $S^{\text{Renyi-2}} = \log(N_c^2)$, the maximum value of EE.

C. EE and flip-flop

In Fig. 23, $S^{\text{Renyi-2}}$ for twisted and planar configurations with $(d, h) = (1, 1)$ (left panel) and $(d, h) = (1, 3)$ (right panel) are compared. Flip-flop due to twisting occurs with $(d, h) = (1, 1)$, and not for $(d, h) = (1, 3)$, which is confirmed based on the analysis conducted thus far. As can be seen in both panels, the flip-flop, the rearrangement of color structure, can be clearly observed as a large change in EE. An entanglement entropy S constructed from a two-body reduced color density matrix ρ is expected to cast light on the internal color confinement structure.

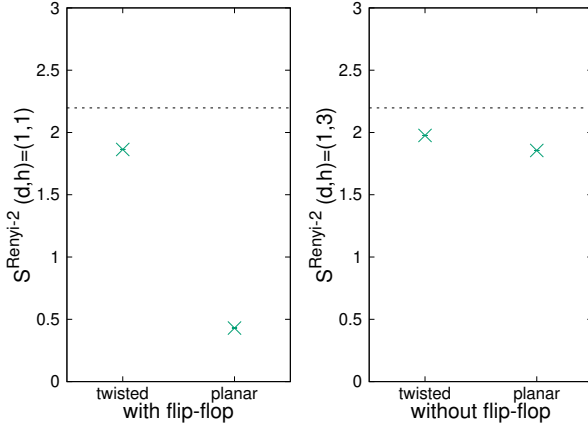


FIG. 23. $S^{\text{Renyi-2}}$ for twisted and planar configurations with $(d, h) = (1, 1)$ and $(1, 3)$, which are measured with Q_1 and \bar{Q}_3 , are shown. The dotted line denotes $S^{\text{Renyi-2}} = \log(N_c^2)$, the maximum value of EE. Flip-flop by twisting occurs with $(d, h) = (1, 1)$, and not for $(d, h) = (1, 3)$.

VI. SUMMARY AND CONCLUDING REMARKS

We have investigated the color correlation between two quarks in static multiquark (NQ) systems in the confined phase by lattice QCD. We have performed quenched lattice QCD calculations with the Coulomb gauge adopting the standard Wilson gauge action, and the spatial volume considered here is $L^3 = 32^3$ at $\beta = 5.8$, which corresponds to the lattice spacing $a = 0.14$ fm and the system volume $L^3 = 4.5^3$ fm 3 . The two-body reduced density matrix ρ in the color space has been constructed from link variables. The calculated ρ has been analyzed based on the ansatz in which the color leak into gluon flux tubes is expressed by mixing of the random density matrix ρ^{rand} as we proposed in our previous papers [10, 12].

Through the whole analyses of 2Q, 3Q and 4Q systems, we have confirmed followings.

- When a system size is small and no gluon flux tube is present, quarks form the “maximally correlated (MC)” color configuration, which is naively expected when we ignore gluon’s color.
- As a system size is enlarged and a long gluon flux tube grows, quarks’ color is screened inside the flux tube, and finally the quarks’ color configuration

approaches the “random” color configuration, in which all the color components equally contribute, as a result of color screening.

- The color configuration of any quark pair can be represented by the color density operator

$$\rho^{\text{ansatz}}(\mathcal{R}) = F_{\text{MC}}(\mathcal{R})\hat{\rho}^{\text{MC}} + (1 - F_{\text{MC}}(\mathcal{R}))\hat{\rho}^{\text{rand}}.$$

$\hat{\rho}^{\text{MC}}$ and $\hat{\rho}^{\text{rand}}$ correspond to the operators for the MC color configuration and the random configuration, respectively. $F_{\text{MC}}(\mathcal{R})$ is the residual rate of the MC color configuration, which is a monotonous function of a flux-tube path length L .

- The flux-tube path length L dependence of the residual rates of the MC color configurations ($F_1^{\text{2Q}}(\mathcal{R})$, $F_3^{\text{3Q}}(\mathcal{R})$, $F_{\bar{3}}^{\text{4Q}}(\mathcal{R})$ and $F_c^{\text{4Q}}(\mathcal{R})$) all retain *universality*; the universal L dependence of the color screening effect along the flux-tube path.
- When two quarks in a pair under consideration belong to different color singlet clusters (mesons), they have no color correlation and their color configuration is expressed by the random color configuration, which can be useful to identify the internal structure of multiquark states.
- The entanglement entropy S defined from the two-body color density matrix ρ can quantify the rearrangement of the internal color structure in multiquark systems.

Possible future directions of this research would be analyses to clarify interquark color correlations as well as color structures and screening effects of flux tubes inside hadrons with dynamical (not static) quarks, inclusion of dynamical sea quarks, etc.

ACKNOWLEDGMENTS

This work was partly supported by Grants-in-Aid of the Japan Society for the Promotion of Science (Grant Nos. 18H05407, 22K03608, 22K03633, 25K07310), and was partly achieved through the use of SQUID at D3 center, Osaka University. The computational resources were provided by RCNP, Osaka University.

[1] J. Greensite, “An Introduction to the Confinement Problem,” Lecture Notes in Physics (Springer, 2011) doi:10.1007/978-3-642-14382-3, and references therein.

[2] G. S. Bali, K. Schilling and C. Schlichter, Phys. Rev. D **51**, 5165 (1995) doi:10.1103/PhysRevD.51.5165 [hep-lat/9409005].

[3] V. G. Bornyakov *et al.* [DIK Collaboration], Phys. Rev. D **70**, 054506 (2004) doi:10.1103/PhysRevD.70.054506 [hep-lat/0401026].

[4] N. Cardoso, M. Cardoso and P. Bicudo, Phys. Rev. D **84**, 054508 (2011) doi:10.1103/PhysRevD.84.054508 [arXiv:1107.1355 [hep-lat]].

[5] G. Tiktopoulos, Phys. Lett. **66B**, 271 (1977). doi:10.1016/0370-2693(77)90878-4

- [6] J. Greensite and C. B. Thorn, JHEP **0202**, 014 (2002) doi:10.1088/1126-6708/2002/02/014 [hep-ph/0112326].
- [7] T. T. Takahashi, H. Suganuma, Y. Nemoto and H. Matsufuru, Phys. Rev. D **65**, 114509 (2002) doi:10.1103/PhysRevD.65.114509 [arXiv:hep-lat/0204011 [hep-lat]].
- [8] F. Okiharu, H. Suganuma and T. T. Takahashi, Phys. Rev. D **72**, 014505 (2005) doi:10.1103/PhysRevD.72.014505 [arXiv:hep-lat/0412012 [hep-lat]].
- [9] F. Okiharu, H. Suganuma and T. T. Takahashi, Phys. Rev. Lett. **94**, 192001 (2005) doi:10.1103/PhysRevLett.94.192001 [arXiv:hep-lat/0407001 [hep-lat]].
- [10] T. T. Takahashi and Y. Kanada-En'yo, Phys. Rev. D **100**, no.11, 114502 (2019) doi:10.1103/PhysRevD.100.114502 [arXiv:1910.00859 [hep-lat]].
- [11] T. T. Takahashi and Y. Kanada-En'yo, Phys. Rev. D **103**, no.3, 034504 (2021) doi:10.1103/PhysRevD.103.034504 [arXiv:2011.10950 [hep-lat]].
- [12] T. T. Takahashi and Y. Kanada-En'yo, Phys. Rev. D **111**, no.1, 014505 (2025) doi:10.1103/PhysRevD.111.014505 [arXiv:2411.13833 [hep-lat]].
- [13] P. Calabrese and J. L. Cardy, J. Stat. Mech. **0406**, P06002 (2004) doi:10.1088/1742-5468/2004/06/P06002 [arXiv:hep-th/0405152 [hep-th]].
- [14] S. Ryu and T. Takayanagi, JHEP **08**, 045 (2006) doi:10.1088/1126-6708/2006/08/045 [arXiv:hep-th/0605073 [hep-th]].
- [15] A. Kitaev and J. Preskill, Phys. Rev. Lett. **96**, 110404 (2006) doi:10.1103/PhysRevLett.96.110404 [arXiv:hep-th/0510092 [hep-th]].
- [16] L. Amico, R. Fazio, A. Osterloh and V. Vedral, Rev. Mod. Phys. **80**, 517-576 (2008) doi:10.1103/RevModPhys.80.517 [arXiv:quant-ph/0703044 [quant-ph]].
- [17] S. N. Solodukhin, Living Rev. Rel. **14**, 8 (2011) doi:10.12942/lrr-2011-8 [arXiv:1104.3712 [hep-th]].
- [18] W. Donnelly, Class. Quant. Grav. **31**, no.21, 214003 (2014) doi:10.1088/0264-9381/31/21/214003 [arXiv:1406.7304 [hep-th]].
- [19] R. Amorosso, S. Syritsyn and R. Venugopalan, JHEP **12**, 177 (2024) doi:10.1007/JHEP12(2024)177 [arXiv:2410.00112 [hep-lat]].